Talanta 116 (2013) 978–984

Contents lists available at ScienceDirect

Talanta

journal homepage: www.elsevier.com/locate/talanta

Magnetically controllable dual-mode nanoprobes for cell imaging with an onion-liked structure

Hui Chen, Zhuyuan Wang, Xueqin Ma, Shenfei Zong, Yiping Cui *

Advanced Photonics Center, Southeast University, Nanjing 210096, Jiangsu, China

ARTICLE INFO

Article history:
Received 9 June 2013
Received in revised form
4 August 2013
Accepted 11 August 2013
Available online 17 August 2013

Keywords:
Surface enhanced Raman scattering
Magnetic
Fluorescence
Onion-liked structure
Multi-mode
Cell imaging

ABSTRACT

A magnetically controllable dual-mode optical probe is demonstrated for cellular imaging with an onion-liked structure, which can exhibit both surface enhanced Raman scattering (SERS) and fluorescence signals. For obtaining such a nanoprobe, Fe_3O_4 nanoparticles were first encapsulated into an inner layer of silica, which were then coated with a second layer of gold nanoshell (designated as Fe_3O_4@SiO_2@Au). By adjusting the thickness of the gold shell, the surface plasmon resonance (SPR) of Fe_3O_4@SiO_2@Au nanoparticles can be easily tuned from visible to near-infrared (NIR) region. Afterwards, the prepared Fe_3O_4@SiO_2@Au nanoparticles were tagged with a third layer of Raman reporters to exhibit SERS signals and further coated with an outmost layer of dye-doped silica to generate fluorescence. When being excited at different wavelengths as 515 nm and 633 nm, the distinct fluorescence and SERS signals can be separately observed. More interestingly, an enhanced cellular uptake of the presented nanoprobes was observed in the presence of a magnetic field, which was proved by both fluorescence and SERS images. This onion-liked multi-modal nanoplatform has great potential in bio-imaging, targeted delivery applications and biological separations.

1. Introduction

Monitoring interactions in living cells is crucial to understand the cellular dynamics or organismal developments for achieving the ultimate goal of cancer therapy. In recent years, fluorescence microscopy has been widely used for real-time, high-speed, and non-invasive imaging of live cells. A large number of fluorophores with distinctive spectral characteristics are available, providing many possibilities for multi-color biological labeling, including organic dyes [1], inorganic nanoparticles [2], lanthanide coordination complexes [3] and bioluminescent proteins [4]. Since the intracellular delivery of organic dyes is relatively easy, organic fluorophores are most commonly used for bio-imaging. However, their relative broad emission profiles sometime limit their applications, especially in those considering multiplex labeling.

Recently, surface enhanced Raman scattering (SERS) spectroscopy has become another powerful method for biomolecular sensing and imaging [5–9]. The richness of SERS spectroscopic information with a high resolution, a much narrower bandwidth and non-photobleaching characteristics make it very intriguing. Up to now, a variety of tailored geometries of nanoparticle-based SERS substrates have been reported, which are mainly composed of gold or silver, including hollow nanospheres [10], nanorods [11,12], nanorings [13] and so on. As one type of the gold nanostructures, gold nanoshells have attracted much attention in recent years. By regulating the relative dimensions between cores and shells, the plasmon resonance of gold nanoshells can be easily tuned from visible to NIR region [14]. More recently, we have developed a kind of dual mode nanoprobe which integrates the fluorescence and SERS signals into a single composite nanoparticle, using organic dyes or quantum dots as the fluorescence generators and gold NPs as the SERS substrates [15,16]. However, the nanoprobes have some limits for *in vivo* imaging because the position and distribution of these probes are random. In fact, controllable nanoparticles have been used in biomolecular and cellular sensing by means of magnetic control tools. Magnetically modulated fluorescent probes have been demonstrated to achieve enhanced cellular uptake of the probes in the presence of a magnetic field *in vitro* [17] and magnetically guided two-photon cellular imaging [18]. So, it is significant that we design a kind of nanoprobe which is not only acts as a standalone SERS substrate with integrated hot-spots or a fluorescence based geometry, but can also be controlled magnetically to produce orientational and translational motion.

Here, we demonstrate a magnetically controllable dual mode optical nanoprobe, which contains a Fe_3O_4 core with multiple layers. For obtaining such a nanoprobe, Fe_3O_4 nanoparticles were first encapsulated into an inner layer of silica, which were then

* Corresponding author. Tel.: +86 25 8379 2470; fax: +86 25 8379 0201.
E-mail address: cyp@seu.edu.cn (Y. Cui).

0039-9140/$ - see front matter © 2013 Elsevier B.V. All rights reserved.
http://dx.doi.org/10.1016/j.talanta.2013.08.015

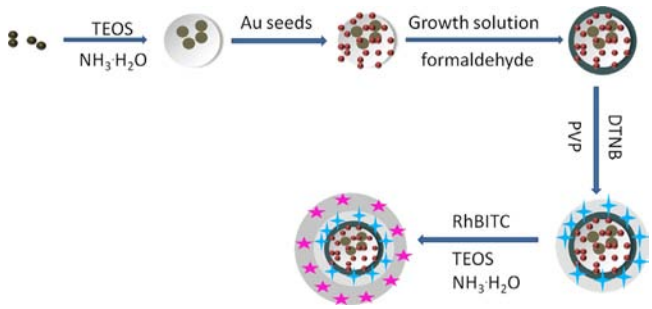

Scheme 1. Schematic representation of the preparation of Fe_3O_4@SiO_2@Au/DTNB@RhBITC/SiO_2 nanocomposites.

coated with a second layer of gold nanoshell. Afterwards, the prepared Fe_3O_4@SiO_2@Au nanoparticles were tagged with a third layer of Raman reporters to exhibit SERS signals and further coated with an outmost layer of dye-doped silica to generate fluorescence. Scheme 1 shows a schematic representation of the synthetic procedure to prepare the magnetic dual-mode nanocomposites. The presented nanoparticles show superparamagnetic properties and dual-mode optical signals as strong fluorescence and intense SERS signals. Our experimental results show that after entering the living cells, the fluorescence and SERS signals of the nanoparticles were well retained and no obvious cytotoxicity was observed. Interestingly, the distribution of nanoprobes in cells could be manipulated through an external magnetic field. Our results indicate that such a kind of multi-mode probe has potential applications in cellular imaging.

2. Experimental section

2.1. Materials

Ferric chloride ($FeCl_3 \cdot 6H2O$) and iron(II) chloride tetrahydrate ($FeCl_2 \cdot 4H_2O$) were purchased from Aladdin. Ammonia solution ($NH_3 \cdot H_2O$), trisodium citrate dehydrate (TSCD), sodium hydroxide (NaOH), absolute ethanol and potassium carbonate (K_2CO_3) were purchased from Shanghai Zhongshi Chemical Co., Ltd. n-Butylamine, and tetraethyl orthosilicate (TEOS) were purchased from Alfa Aesar. (3-Aminopropyl)triethoxysilane (APTES), hydrogen tetrachloroaurate(III) trihydrate ($HAuCl_4 \cdot 3H_2O$), tetrakis(hydroxymethyl) phosphonium chloride solution (THPC), (3-aminopropyl) trimethoxysilane (APTMS), 5,5′-dithiobis-(2-nitrobenzoic acid) (DTNB) and rhodamine B isothiocyanate (RhBITC) were purchased from Sigma-Aldrich. All the reagents were used as received. Deionized water (Millipore Milli-Q grade) with resistivity of 18.2 MΩ was used in all the experiments.

2.2. Fabrication of Fe_3O_4@SiO_2 nanospheres

First, Fe_3O_4 nanoparticles were prepared by the co-precipitation method [19]. Then, a layer of silica was coated on the surfaces of Fe_3O_4 nanoparticles by the Stöber process [20,21]. Briefly, 1 g of $FeCl_2 \cdot 4H_2O$ and 2.7 g of $FeCl_3 \cdot 6H_2O$ were mixed in 40 mL of water and heated to 80 °C under argon in a three-necked flask. While vigorously stirring the reaction mixture, 6 mL of $NH_3 \cdot H_2O$ was introduced by a syringe, and the heating was continued for 30 min. After that, 4 g of TSCD in 10 mL water was added and the temperature was increased to 90 °C while stirring was continued for an additional 90 min. The Fe_3O_4 precipitates were separated centrifugally at 12,000 rpm for 10 min and washed three times with deionized water. Then, the precipitate was re-dispersed in 10 mL of water.

Silica coated Fe_3O_4 nanoparticles were prepared by the hydrolysis of TEOS using the Stöber method. In a typical experiment, 60 μL of the as-prepared Fe_3O_4 aqueous solution were added to the mixture of 25 mL of ethanol and 4 mL water under vigorous stirring, and then 0.60 mL of $NH_3 \cdot H_2O$ solution was added. 5 min later, 0.60 mL of TEOS were added dropwise and the mixture solution was stirred overnight. Then, the silica coated Fe_3O_4 nanoparticles were obtained and the thickness of the silica coating can be controlled by changing the amount of TEOS.

2.3. Synthesis of Fe_3O_4@SiO_2@Au nanocomposites

Fe_3O_4@SiO_2@Au nanocomposites were prepared according to the method of Liu et al. [22]. First, gold seeds were adsorbed to the surfaces of APTES-functionalized silica (Fe_3O_4@SiO_2–APTES), nanoshells were then grown by reacting the seed particles with $HAuCl_4$ in the presence of a reducing agent, such as formaldehyde, to produce a smooth and uniform gold layer.

To prepare gold seeds of 1–3 nm in diameter, 0.5 mL of 1 M NaOH and 12 μL of THPC in 1 mL water were mixed with 50 mL of deionized water, and 2.0 mL of 1% $HAuCl_4$ was added quickly to the mixed solution [23]. The colloid solution was stored in a refrigerator maintained at 4 °C for 5–30 day.

To prepare the APTES-modified silica core particles (Fe_3O_4@-SiO_2–APTES), an excess of APTES (300 μL) was added to 10 mL of the ethanol solution of Fe_3O_4@SiO_2 core particles with vigorous stirring for 2 h. To enhance the covalent bonding of the APTES groups to the silica surfaces, the solution was diluted to 100 mL and gently stirred at 70 °C for 1 h. After several times of centrifugations, Fe_3O_4@SiO_2–APTES was redispersed in 10 mL of ethanol.

To attach the gold nanoparticles, 3.0 mL of the Fe_3O_4@SiO_2–APTES particles was added to the concentrated gold colloids and mixed thoroughly. The resulting Fe_3O_4@SiO_2@Au-seeds (seed particles) were washed by centrifugation and redispersed by an ultrasonic bath in 10 mL of water.

For growing the gold nanoshell on the seed particles, a solution of 25 mg of anhydrous potassium carbonate was added to 100 mL of water containing 1.5 mL of 1% $HAuCl_4$ solution, which is called PCG in short. To determine the effect of PCG on the formation of gold nanoshells, different amounts of PCG were rapidly stirred with 1 mL of the seed solution followed by the addition of the formaldehyde solution. The resultant nanoparticles were washed by centrifugation and re-dispersed in water.

2.4. Synthesis of Fe_3O_4@SiO_2@Au/DTNB@RhBITC/SiO_2 nanocomposites

Fe_3O_4@SiO_2@Au/DTNB@RhBITC/SiO_2 nanoparticles were fabricated through a modified Stöber method. SERS-activated Fe_3O_4@-SiO_2@Au/DTNB complex was pre-prepared by adding 12 μL of 10^{-2} M DTNB into 5 mL of Fe_3O_4@SiO_2@Au solution. 2 h later, 1 mL of PVP solution (30 mg/mL) was added and then reacted for another 12 h under continuous stirring [24]. The resultant Fe_3O_4@-SiO_2@Au/DTNB@PVP nanoparticles were washed by centrifugation and re-dispersed in ethanol. Then, in a typical experiment, 5 mL of the as-prepared Fe_3O_4@SiO_2@Au/DTNB solution was added with 11 mL of ethanol and 4 mL of water, followed by the successive addition of RhBITC–APTES complex, 20 μL of TEOS and 190 μL of ammonium hydroxide. The mixture was continuously stirred for 5 h. Here, the RhBITC–APTES complex was pre-prepared by adding 5 μL of APTES solution to 100 μL of RhBITC solution in ethanol, which was then reacted for 12 h in dark under continuous stirring. Finally, the as-prepared composite magnetic dual mode nanoparticles were washed by centrifugation and re-dispersed in ethanol.

2.5. Instruments

Extinction spectra were measured by a Shimadzu UV-3600 PC spectrophotometer with quartz cuvettes of 1 cm path length. Photoluminescence emission spectra were measured by an Edinburgh FLS920 spectro-fluorimeter. Transmission electron microscope (TEM) images were obtained with an FEI Tecnai G^2T20 electron microscope operating at 200 kV. SERS and fluorescence measurements were performed with a confocal microscope (FV1000, Olympus). Fluorescence images of the cells were recorded at 515 nm excitation, and SERS spectra were obtained at 633 nm excitation. The laser power was 2.3 mW at the sample position. Rayleigh scattering light was removed by a holographic notch filter. The Raman scattering light was directed to an Andor shamrock spectrograph equipped with a charge-coupled device (CCD).

3. Results and discussion

The typical morphologies, structures, and dispersivity of Fe_3O_4@SiO_2 were analyzed by TEM images. As shown in Fig. 1a, the average size of Fe_3O_4@SiO_2 nanoparticles is about 140 nm. It is worth noting that for the successful adsorption of the gold seeds to Fe_3O_4@SiO_2–APTES, the surface electric properties of Fe_3O_4@SiO_2 nanoparticles and pH value of the gold seeds solution are crucial. Therefore, an excess amount of APTES is required to offer enough amino groups to saturate the surfaces of the silica cores and subsequently led to a uniform attachment of the gold seeds which show a small SPR band (Fig. S1, Supporting information). The TEM image of Fe_3O_4@SiO_2 absorbed with gold seeds is shown in Fig. 1b. It can be seen that the gold seeds have been uniformly attached on the surfaces of Fe_3O_4@SiO_2 spheres.

Further, to grow a complete gold shell, $HAuCl_4$ was reduced by formaldehyde and deposited on the gold seeds, which serve as the nucleation sites during the formation of rough gold nanoshell. In our experiments, different volumes of the freshly prepared PCG solution and 0.5 mL of the seed solution were mixed and stirred for 10 min, and then a fixed amount of formaldehyde solution as 200 μL of 37% formaldehyde was added. Over the first course of 10–30 min, the solution changed from colorless to blue, which is the characteristic of the formation of nanoshells. The extinction spectra of different batches of Fe_3O_4@SiO_2@Au nanoparticles are shown in Fig. 2a, which were prepared with different amounts of PCG solutions during the experiments. With the increased amount of PCG from 10 to 80 mL, the extinction peak experienced a red shift. And the extinction spectrum peaks at around 750 nm when 80 mL of PCG solution was used. TEM images of the formed nanoshells using different volumes of PCG as 10, 30, 60 and 80 mL, respectively, are shown in Fig. 3a, b, c and d. It can be seen that the shell growth was gradually completed on the silica particle surfaces with increased volume of PCG solution. Specifically, in our experiments, the shell growth was almost complete when 80 mL of PCG solution was used. The thicknesses of the gold shells was about 10 nm, 13 nm, 15 nm, and 20 nm calculated from

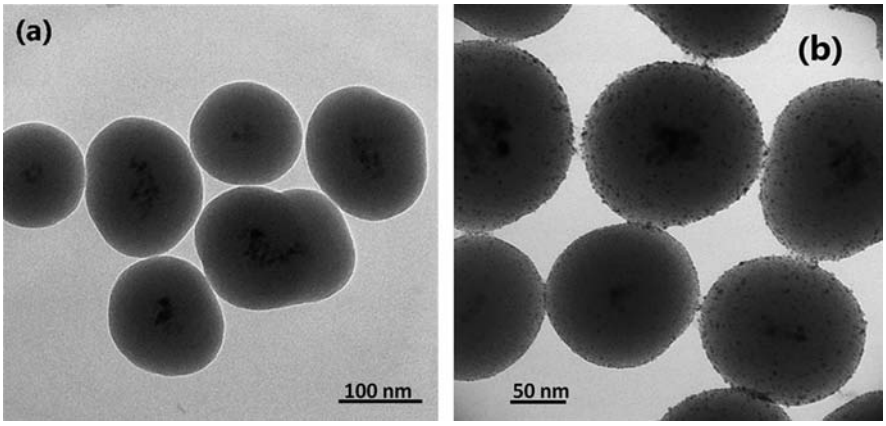

Fig. 1. TEM images of (a) Fe_3O_4@SiO_2 nanoparticles with a core diameter of about 140 nm and (b) Fe_3O_4@SiO_2 absorbed with gold seeds.

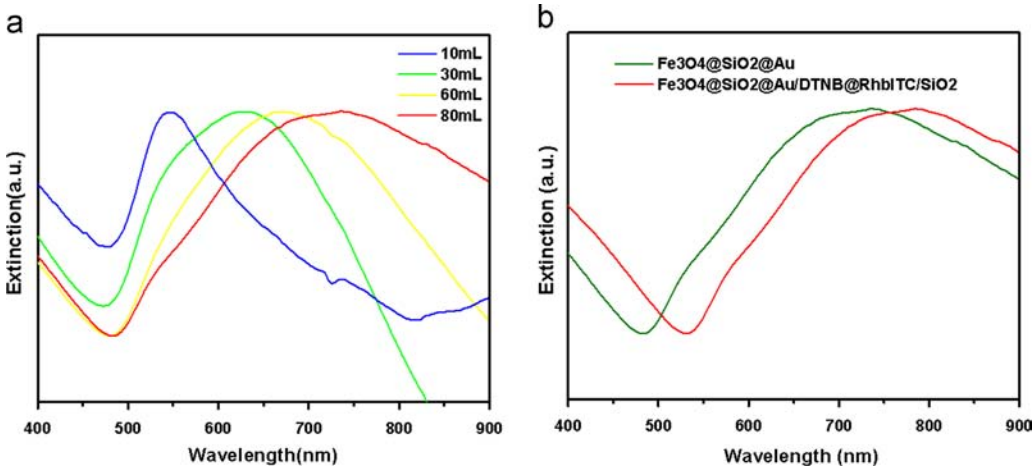

Fig. 2. (a) Extinciton spectra of the Fe_3O_4@SiO_2@Au nanoparticles, which were prepared with 10 mL, 30 mL, 60 mL, and 80 mL of the freshly prepared PCG solution. The volume of the seed solution was fixed as 1 mL. (b) Extinction spectra of $Fe3O_4$@SiO_2@Au and Fe_3O_4@SiO_2@Au/DTNB@RhBITC/SiO_2.

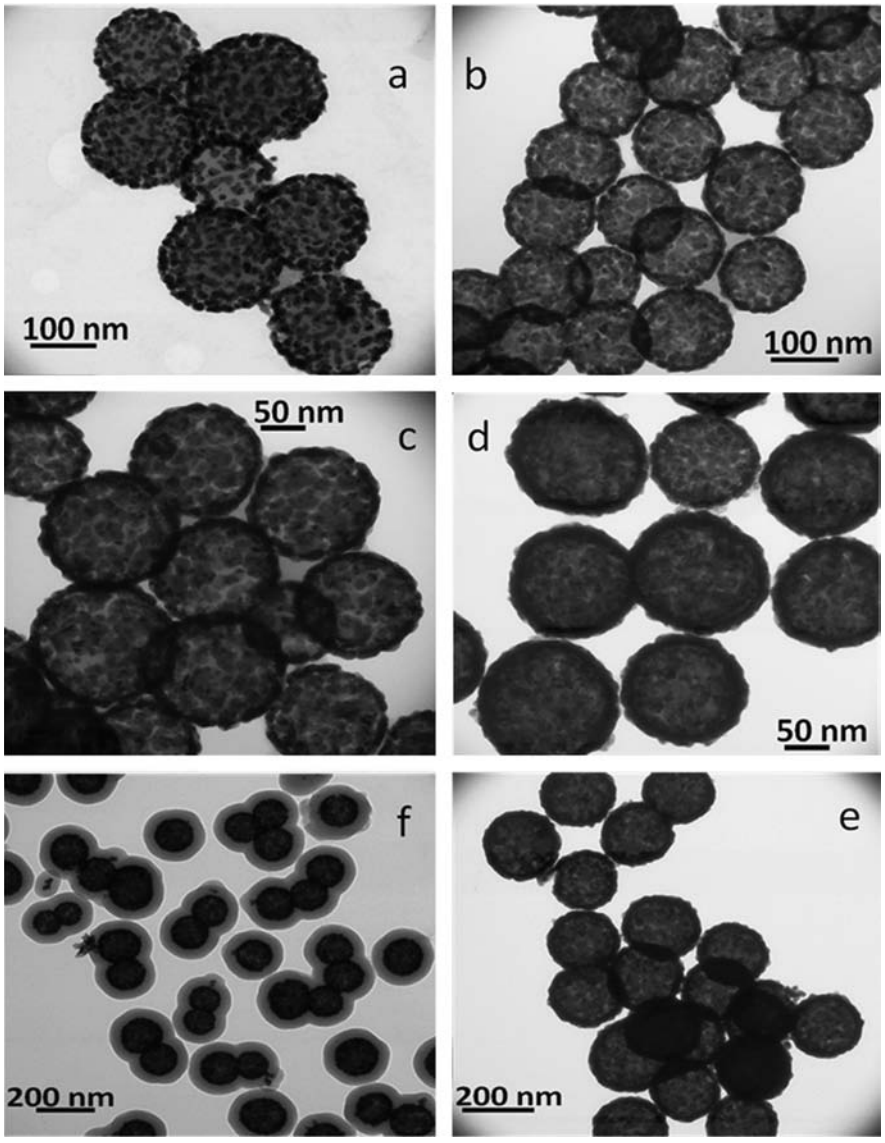

Fig. 3. TEM images of the Fe_3O_4@SiO_2@Au nanoparticles using (a) 10 mL; (b) 30 mL; (c) 60 mL; (d) 80 mL of PCG solution. The volume of added seed solution was fixed as 0.5 mL. TEM images of (e) Fe_3O_4@SiO_2@Au and (f) Fe_3O_4@SiO_2@Au/DTNB@RhBITC/SiO_2 nanoparticles.

the TEM image in Fig. 3a, b, c and d, respectively. Further increase of PCG only increased the shell thickness, which led to a blue-shift of the maximum peak in the extinction spectra.

Then, DTNB molecules were adsorbed on the surfaces of the gold nanoshells through Au–S bonds to generate SERS signals. Many approaches can be used to investigate the interaction of gold and thiol groups [25–31]. More exactly, upon interaction with gold nanoshells, DTNB molecules tend to dissociate into two 2-nitro-5-thiobenzoate (TNB), which will be spontaneously immobilized onto the surface of gold via thiol groups (Fig. S2, Supporting information) [32–35]. The SERS spectrum is shown in Fig. 4a, which is characterized by peaks at 1333, 1067, 1152, and 1558 cm^{-1}, assigned to the symmetric stretch of the nitro groups, the succinimidyl N–C–O stretch overlapping with aromatic ring modes, the C–H deformation modes and the aromatic ring C–C stretching modes, respectively [16].The SERS spectra (shown in Fig. 4a) of DTNB-tagged gold nanoshells with a structure in Fig. 3a, b, and d, are shown. It can be observed that the intensities of SERS signals differ with different thicknesses of nanoshells. Specifically, the intensity of SERS signals increases as the growth of the gold nanoshell gradually completes. This is reasonable since more hotspots are presented on the complete gold nanoshell. In our following experiments, gold nanoshells with a structure shown in Fig. 3d were employed due to its stronger SERS signals.

Further, to obtain a SERS and fluorescence dual mode probe, the as-prepared SERS-activated Fe_3O_4@SiO_2@Au/DTNB nanoparticles were coated with a layer of RhBITC-doped silica shells. The TEM images (shown in Fig. 3f) of Fe_3O_4@SiO_2@Au/DTNB@RhBITC/SiO_2 nanoparticles, which exhibit a spherical shape as well as a uniform size. The thickness of the silica shell can be tuned by changing the amount of tetraethyl orthosilicate (TEOS) or the amount of ammonia solution. In our experiments, the thickness of the silica-shell is 40 nm on average and an average diameter of Fe_3O_4@SiO_2@Au/DTNB@RhBITC/SiO_2 NPs is about 260 nm. Moreover, after the silica coating process, the SPR band of the Fe_3O_4@SiO_2@Au NPs red-shifted from 750 nm to 798 nm as shown in Fig. 2b. This is reasonable since the silica layer increased the refractive index around the gold nanoshells [36]. As shown in Fig. 4b, Fe_3O_4@SiO_2@Au/DTNB@RhBITC/SiO_2 exhibits representative Raman bands of DTNB molecules which were well assigned previously. After the gold shell being coated with RhBITC-doped silica layer, the SERS spectra of the probes remained well except that the intensity decreased a little. On the other hand, the fluorescence of RhBITC was also kept strong after being doped

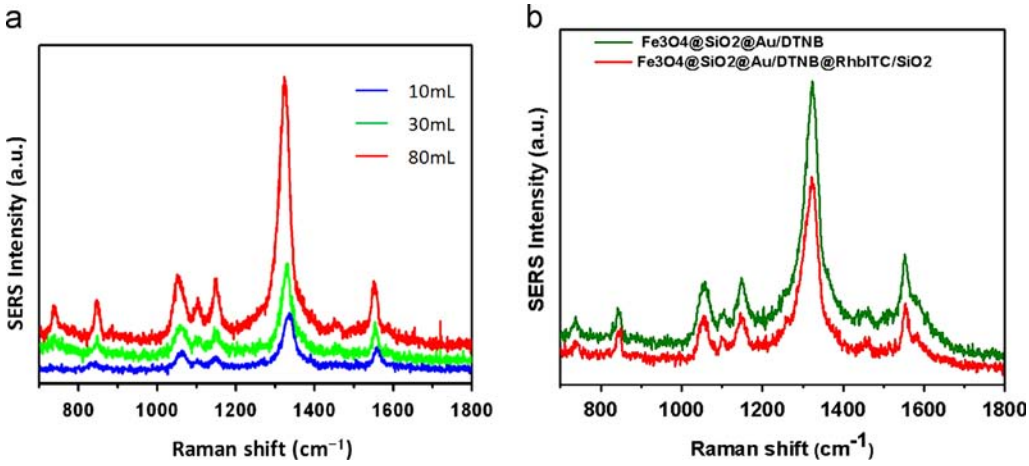

Fig. 4. (a) SERS spectra of Fe_3O_4@SiO_2@Au nanocomposites using DTNB as SERS reporters. Gold nanoshells with different thicknesses obtained using different volumes of PCG as 10 mL, 30 mL, and 80 mL. (b) SERS spectra of Fe_3O_4@SiO_2@Au/DTNB and Fe_3O_4@SiO_2@Au/DTNB@RhBITC/SiO_2 nanoparticles.

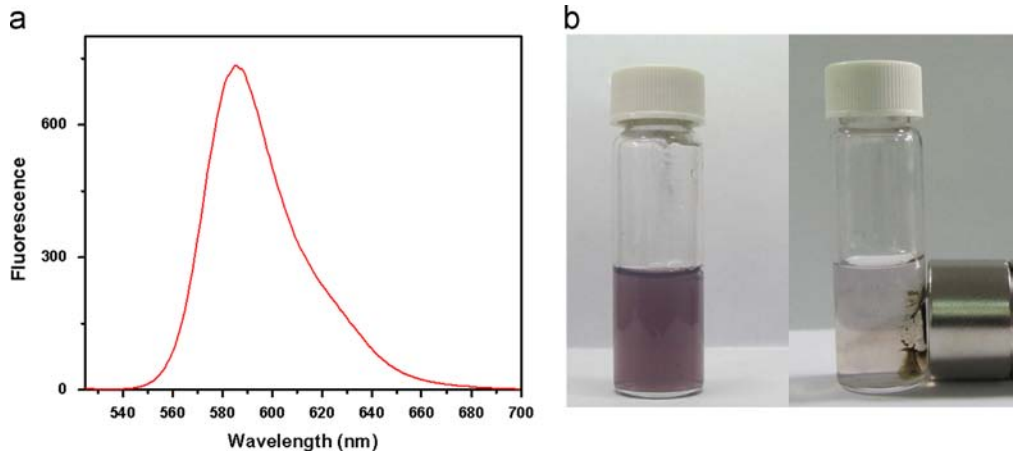

Fig. 5. (a) PL spectrum of Fe_3O_4@SiO_2@Au/DTNB@RhBITC/SiO_2, the excitation wavelength was 515 nm. (b) Photographs of Fe_3O_4@SiO_2@Au/DTNB@RhBITC/SiO_2 solution (left) before and (right) with and without an external magnetic field.

inside the outer silica shell, as shown in Fig. 5a. This benefits from the PVP layer which blocks the possible contact between RhBITC and gold shells. In addition, since the outer silica shell is very thick (about 40 nm) while usually the effective distance of quenching between dye and metal is about 10 nm and RhBITC was uniformly doped in it, even the fluorescence of RhBITC close to gold nanoshells was quenched, the overall fluorescence of the nanocomposites was still observed which is strong enough to be used for fluorescence imaging. To further prove this, the silica thickness dependent fluorescence quenching was investigated (Fig. S3).

To investigate the magnetization of the Fe_3O_4@SiO_2@Au nanoprobes, an external magnetic field was employed. As shown in Fig. 5b, these Fe_3O_4@SiO_2@Au nanoparticles were aggregated under an external magnetic field within 2 h, which indicates of the superparamagnetic characteristics of the hybrid NPs. For a comparative study, the magnetic activity of the individual Fe_3O_4 NPs was also investigated under an external magnetic field. The result shows that Fe_3O_4 NPs aggregated in a shorter period of time as 30 min. This indicates that the magnetization of Fe_3O_4 was reduced after being coated with a gold nanoshell. For obtaining a stronger magnetization, more Fe_3O_4 aggregates or large magnetic sphere could be employed.

Finally, to investigate the magnetic targeting ability of such a dual mode nanoparticle in living cells, a cellular culture system including both control and magnetic targeting sites was used as shown in Fig. 6a. In the experiments, HeLa cells were incubated with Fe_3O_4@SiO_2@Au/DTNB@RhBITC/SiO_2 NPs for 2 h and washed with phosphate-buffered saline (PBS) before SERS and fluorescence imaging. Besides, a magnetic field was obtained by fixing a magnet under the cultural dish. HeLa cells localized within both the control and the targeting sites were subject to the same cell culture conditions. As shown in Fig. 6, both fluorescence images and SERS mapping show that the concentration of Fe_3O_4@SiO_2@Au/DTNB@RhbITC/SiO_2 NPs at the targeting side was higher than that at control site. Specially, stronger fluorescence (Fig. 6c) and SERS signals (Fig. 6e) were observed on the plasma membranes of HeLa cells at the magnetic targeting sites, indicating that a large number of Fe_3O_4@SiO_2@Au/DTNB@RhBITC/SiO_2 composites have been delivered into cells after 2 h of incubation. However, only minor traces of fluorescence (Fig. 6b) and SERS signals (Fig. 6d) were detected in HeLa cells at the control sites. For a more accurate comparison, the SERS spectra collected from the spots located in control and targeting sites were shown in Fig. 6d and e. The SERS intensity acquired from the targeting spot is about three times of that measured from the control spot. The above experimental results indicate the good magnetic targeting ability of such a dual-mode probe. Thus, this presented nanoprobe has great potential in bio-imaging due to its strong fluorescence, distinct SERS signals and good magnetic response.

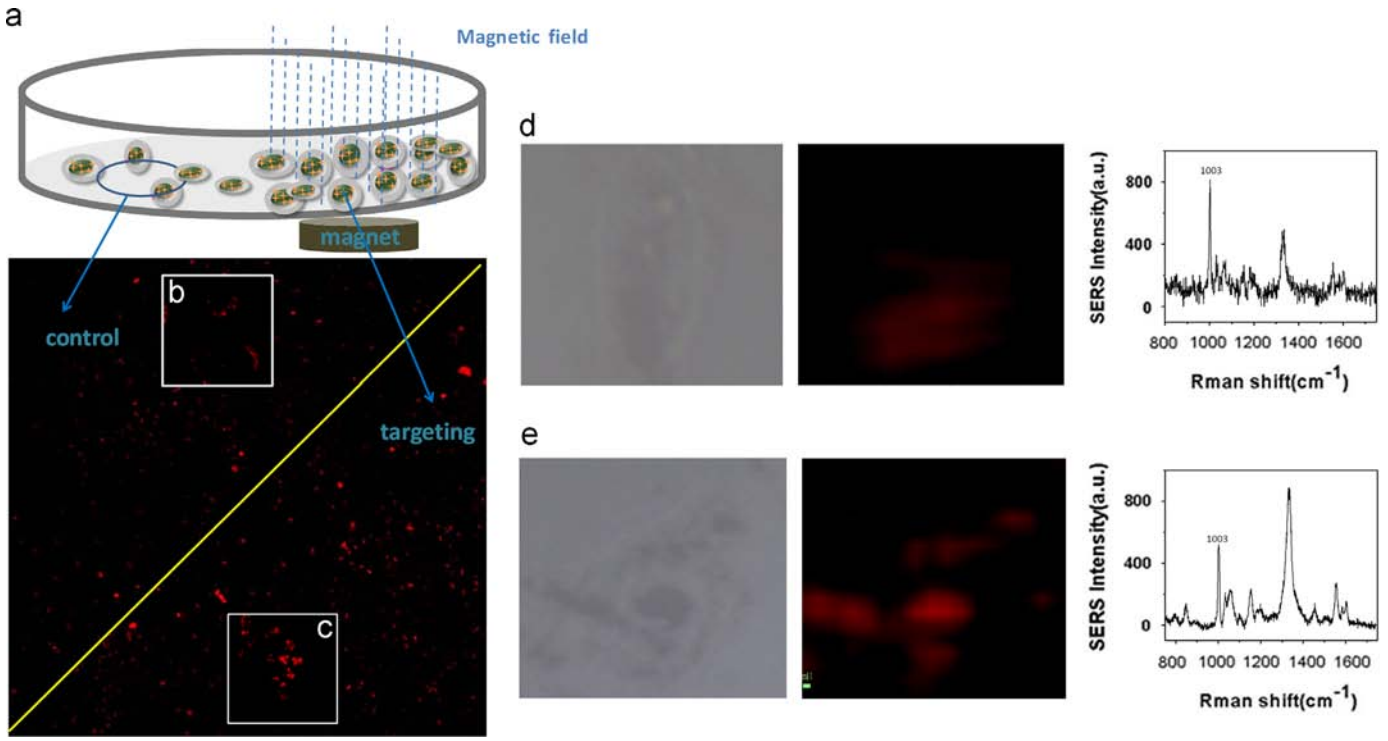

Fig. 6. The magnetic targeting studies using HeLa cells incubated with magnetic dual-mode probes at 37 °C for 2 h. (a) Fluorescence image in the regions of both control site and targeting site. The insets (b) and (c) show the enlarged ones of control and target sites, respectively; (d) SERS mapping, SERS spectrum and the bright-field image of HeLa cells at the control site; and (e) SERS mapping, SERS spectrum and the bright-field image of HeLa cells at the targeting site. The excitation wavelengths for fluorescence images and SERS spectra were 515 and 633 nm, respectively. The SERS peak at 1003 cm^{-1} belongs to the bottom of the culture dish.

4. Conclusion

A kind of magnetically responsive multimode nanoprobes has been developed with an onion-liked structure. Due to the multi-layered structure, the strong fluorescence and SERS signals of the nanoprobes can be well retained without being disturbed from each other. Besides, by selecting different Raman reporters or fluorescent agents in corresponding layers, various combinations of optical signals can be easily achieved, which is important for multiplexed bio-sensing or bio-imaging. Moreover, by integrating superparamagnetism characteristics, this nanoprobe can be magnetically guided to label specific living cells under a magnetic field. Thus, this kind of integrated nanoplatform would have a great potential in the investigation of cellular dynamics or organismal developments, targeted drug delivery and biological separations.

Acknowledgments

This work was supported by Natural Science Foundation of China (NSFC) (Nos. 60708024, 60877024, 61177033, and 21104009), the Specialized Research Fund for the Doctoral Program of Higher Education (SRFDP) (Nos. 20070286058 and 20090092110015), the Science Foundation for The Excellent Youth Scholars of Southeast University, the Scientific Research Foundation of Graduate School of Southeast University (YBJJ1125), and the Fundamental Research Funds for the Central Universities.

Appendix A. Supplementary material

Supplementary data associated with this article can be found in the online version at http://dx.doi.org/10.1016/j.talanta.2013.08.015.

References

[1] C.H. Lee, S.H. Cheng, Y.J. Wang, Y.C. Chen, N.T. Chen, J. Souris, C.T. Chen, C.Y. Mou, C.S. Yang, L.W. Lo, Adv. Funct. Mater. 19 (2009) 215–222.
[2] X.H. Gao, Y.Y. Cui, R.M. Levenson, L.W.K. Chung, S.M. Nie, Nat. Biotechnol. 22 (2004) 969–976.
[3] X.W. Yan, L.M. Yang, Q.Q. Wang, Angew. Chem. Int. Ed. 50 (2011) 5130–5133.
[4] A.M. Pavlov, G.B. Sulchorukov, D.J. Gould, Biomacromolecules 14 (2013) 608–612.
[5] H. Park, S. Lee, L. Chen, E.K. Lee, S.Y. Shin, Y.H. Lee, S.W. Son, C.H. Oh, J.M. Song, S.H. Kang, J. Choo, Phys. Chem. Chem. Phys. 11 (2009) 7444–7449.
[6] C. Song, Z. Wang, R. Zhang, J. Yang, X. Tan, Y. Cui, Biosens. Bioelectron. 25 (2009) 826–831.
[7] G. von Maltzahn, A. Centrone, J.H. Park, R. Ramanathan, M.J. Sailor, T.A. Hatton, S.N. Bhatia, Adv. Mater. 21 (2009) 3175–3180.
[8] Y.G. Sun, Y.N. Xia, Anal. Chem. 74 (2002) 5297–5305.
[9] S.F. Zong, Z.Y. Wang, J. Yang, Y.P. Cui, Anal. Chem. 83 (2011) 4178–4183.
[10] M. Sanles-Sobrido, W. Exner, L. Rodriguez-Lorenzo, B. Rodriguez-Gonzalez, M.A. Correa-Duarte, R.A. Alvarez-Puebla, L.M. Liz-Marzan, J. Am. Chem. Soc. 131 (2009) 2699–2705.
[11] Z. Wang, S. Zong, J. Yang, C. Song, J. Li, Y. Cui, Biosens. Bioelectron. 26 (2010) 241–247.
[12] S.J. Oldenburg, S.L. Westcott, R.D. Averitt, N.J. Halas, J. Chem. Phys. 111 (1999) 4729–4735.
[13] X. Ji, R. Shao, A.M. Elliott, R.J. Stafford, E. Esparza-Coss, J.A. Bankson, G. Liang, Z.-P. Luo, K. Park, J.T. Markert, C. Li, J. Phys. Chem. C 111 (2007) 6245–6251.
[14] Q.F. Chen, Y.Y. Rao, X.Y. Ma, J.A. Dong, W.P. Qian, Anal. Methods 3 (2011) 274–279.
[15] Z.Y. Wang, S.F. Zong, J. Yang, J. Li, Y.P. Cui, Biosens. Bioelectron. 26 (2011) 2883–2889.
[16] Z.Y. Wang, S.F. Zong, H. Chen, H. Wu, Y.P. Cui, Talanta 86 (2011) 170–177.
[17] F. Erogbogbo, K.T. Yong, R. Hu, W.C. Law, H. Ding, C.W. Chang, P.N. Prasad, M.T. Swihart, ACS Nano 4 (2010) 5131–5138.
[18] Q. Zheng, T.Y. Ohulchanskyy, Y. Sahoo, P.N. Prasad, J. Phys. Chem. C 111 (2007) 16846–16851.
[19] Y. Sahoo, A. Goodarzi, M.T. Swihart, T.Y. Ohulchanskyy, N. Kaur, E.P. Furlani, P.N. Prasad, J. Phys. Chem. B 109 (2005) 3879–3885.
[20] W. Stober, A. Fink, E. Bohn, J. Colloid Interface Sci. 26 (1968) 62.
[21] P. Lange, A. Schier, H. Schmidbaur, Inorg. Chem. 35 (1996) 637–642.
[22] S.Y. Liu, Z.S. Liang, F. Gao, J.H. Yu, S.F. Luo, N.C. Jesus, G.Q. Lu, Chin. J. Chem. 27 (2009) 1079–1085.
[23] D.G. Duff, A. Baiker, P.P. Edwards, Langmuir 9 (1993) 2301–2309.
[24] S.F. Zong, Z.Y. Wang, H. Chen, J. Yang, Y.P. Cui, Anal. Chem. 85 (2013) 2223–2230.

[25] J. Akola, M. Walter, R.L. Whetten, H. Hakkinen, H. Gronbeck, J. Am. Chem. Soc. 130 (2008) 3756.
[26] M.W. Heaven, A. Dass, P.S. White, K.M. Holt, R.W. Murray, J. Am. Chem. Soc. 130 (2008) 3754.
[27] P.D. Jadzinsky, G. Calero, C.J. Ackerson, D.A. Bushnell, R.D. Kornberg, Science 318 (2007) 430–433.
[28] O. Lopez-Acevedo, H. Tsunoyama, T. Tsukuda, H. Hakkinen, C.M. Aikens, J. Am. Chem. Soc. 132 (2010) 8210–8218.
[29] H.F. Qian, M.Z. Zhu, Z.K. Wu, R.C. Jin, Acc. Chem. Res. 45 (2012) 1470–1479.
[30] J.B. Tracy, M.C. Crowe, J.F. Parker, O. Hampe, C.A. Fields-Zinna, A. Dass, R.W. Murray, J. Am. Chem. Soc. 129 (2007) 16209–16215.
[31] O. Varnavski, T. Goodson, L. Sukhomlinova, R. Twieg, J. Phys. Chem. B 108 (2004) 10484–10492.
[32] C.W. Chang, J.D. Liao, H.C. Chang, L.K. Lin, Y.Y. Lin, C.C. Weng, J. Colloid Interface Sci. 358 (2011) 384–391.
[33] D.S. Grubisha, R.J. Lipert, H.Y. Park, J. Driskell, M.D. Porter, Anal. Chem. 75 (2003) 5936–5943.
[34] A. Michota, J. Bukowska, J. Raman Spectrosc. 34 (2003) 21–25.
[35] Z.Y. Wang, S.F. Zong, J. Yang, C.Y. Song, J. Li, Y.P. Cui, Biosens. Bioelectron. 26 (2010) 241–247.
[36] C.-D. Chen, S.-F. Cheng, L.-K. Chau, C.R.C. Wang, Biosens. Bioelectron. 22 (2007) 926–932.